Imaging Single Endocytic Events Reveals Diversity in Clathrin, Dynamin and Vesicle Dynamics

Alexa L. Mattheyses[1,2,†], Claire E. Atkinson[1,†] and Sanford M. Simon[1,*]

[1]*Laboratory of Cellular Biophysics, The Rockefeller University, New York, NY 10065, USA*
[2]*Present address: Department of Cell Biology, Emory University School of Medicine, Atlanta, GA 30322, USA*
Corresponding author: Sanford M. Simon, simon@rockefeller.edu
[†]*These authors contributed equally to this work.*

The dynamics of clathrin-mediated endocytosis can be assayed using fluorescently tagged proteins and total internal reflection fluorescence microscopy. Many of these proteins, including clathrin and dynamin, are soluble and changes in fluorescence intensity can be attributed either to membrane/vesicle movement or to changes in the numbers of individual molecules. It is important for assays to discriminate between physical membrane events and the dynamics of molecules. Two physical events in endocytosis were investigated: vesicle scission from the plasma membrane and vesicle internalization. Single vesicle analysis allowed the characterization of dynamin and clathrin dynamics relative to scission and internalization. We show that vesicles remain proximal to the plasma membrane for variable amounts of time following scission, and that uncoating of clathrin can occur before or after vesicle internalization. The dynamics of dynamin also vary with respect to scission. Results from assays based on physical events suggest that disappearance of fluorescence from the evanescent field should be re-evaluated as an assay for endocytosis. These results illustrate the heterogeneity of behaviors of endocytic vesicles and the importance of establishing suitable evaluation criteria for biophysical processes.

Key words: clathrin, dynamin, endocytosis, Epi-TIR, TIRF, total internal reflection microscopy

Clathrin-mediated endocytosis is critical for a number of biological processes including the internalization of nutrients, growth factors and receptors into cells. This process involves assembly and maturation of clathrin-coated pits into endocytic vesicles and requires the coordination of multiple events. This process involves recruitment of clathrin and other cytosolic proteins to the plasma membrane, incorporation of transmembrane receptors, formation of a vesicle through invagination of the plasma membrane and scission of the vesicle from the plasma membrane (1,2). The nascent vesicle is then trafficked into the cell and the clathrin coat is removed (3).

Many proteins and phospholipids contribute to the formation of the vesicle, affect membrane curvature and facilitate recruitment of cargo. However, the timing of recruitment of these molecules relative to physical events is still largely unresolved (4).

Clathrin-mediated endocytosis can be studied in live cells using fluorescent fusion proteins and total internal reflection (TIR) fluorescence microscopy, allowing identification and analysis of individual clathrin-coated pits on the cell surface (5,6). At the plasma membrane, clathrin has been observed to display a variety of behaviors including disappearance, lateral movement, fission and fusion of spots and long-term stasis (7). The lifetimes of clathrin puncta at the membrane are variable, ranging from seconds to several minutes (8–10).

Other endocytic proteins also show heterogeneous behaviors: the time between disappearance of the adaptor complex AP2 and clathrin from the membrane is variable, epsin is present on two-thirds of internalizing vesicles (7), and G- proteins have been shown to localize only a subset of clathrin-coated pits (11). However, the significance of these differences with respect to the underlying biophysical processes of vesicle formation and internalization remains unclear.

TIR has proved particularly powerful in the study of endocytosis, because it provides a spatially selective excitation field, the evanescent field, which penetrates approximately 100 nm into the sample (12). The evanescent field therefore excites only molecules at or near the cell membrane, significantly enhancing the signal-to-noise (S/N) ratio by eliminating out-of-focus fluorescence. The evanescent field depth is approximately the same as the diameter of an endocytic vesicle, facilitating observation of endocytic dynamics. Typically, in these studies, the loss of clathrin fluorescence at the membrane is interpreted as an endocytic event. However, many endocytic proteins, including clathrin, are cytosolic and can potentially associate with or dissociate from the vesicle at any time. It is not possible to determine whether the disappearance of fluorescence signal of a labeled cytosolic protein from the evanescent field of is due to vesicle internalization, dissociation of the protein from the membrane or a change in fluorophore orientation relative to the polarized evanescent field.

TIR has been used to examine the dynamics of single vesicles, yielding information that is lost in bulk assays and population averages. Different criteria have been

utilized to identify subsets of clathrin puncta for analysis. These have included the residence time of clathrin at the cell membrane, a requirement for diffraction-limited clathrin puncta, limited lateral movement of the puncta, the exponential decay of clathrin fluorescence and colocalization of clathrin fluorescence with fluorescence of another endocytic marker (5,6,8,13). Alternately, particle tracking software combined with statistical methods offer the potential to analyze most puncta (9). This diversity in criteria has lead to multiple models for endocytic dynamics, which may be based on different subsets of vesicle behaviors.

A number of studies have examined the dynamics of different proteins during endocytosis. Fluorescence microscopy has been used to study clathrin deformation and movement into the cell (13), as well as scission from the plasma membrane. The relationship between the fluorescent protein signals and the biophysical events which are common to all endocytosed vesicles including membrane deformation, neck constriction, vesicle scission and vesicle internalization are currently unclear (14). In addition to measuring the dynamics of fluorescent proteins relative to each other, it is important to relate protein dynamics to physical events.

Axial movements of exocytic vesicles have been assayed by changes in intensity in TIR microscopy (15). This method was appropriate because the number of fluorophores inside exocytic vesicles was unchanging. In endocytosis, such measurements are more challenging because the number of fluorophores may be changing at the same time as axial movements. Nonetheless, several techniques to investigate physical events have have been published. Sequential epi and TIR illumination (epi-TIR) have been used by several groups to investigate internalization of vesicles (14,16,17). Notably, these studies looked only at clathrin and cytosolic proteins. DiNa, a technique also based on epi-TIR, was developed to study nanometer axial movements of clathrin deformation and internalization (13). The scission of the vesicle from the plasma membrane has been detected with a pH-sensitive tag in an assay that is applied here (5).

In this article, we show that both clathrin and dynamin exhibit a variety of behaviors during endocytosis and that averaging the fluorescence from different vesicles can mask these differences. We utilize histograms to display and evaluate the distribution of endocytic behaviors. Using tools to identify productive endocytic events, we show that clathrin uncoating occurs at variable times relative to vesicle internalization. Clathrin and dynamin are present during vesicle scission from the plasma membrane but remain on the vesicle following scission for variable times. These results show a diversity of behaviors of molecules relative to physical events. At the same time, they emphasize the importance of establishing criteria for evaluating both physical events and protein dynamics.

Results

Population dynamics of clathrin and dynamin

To investigate clathrin and dynamin behaviors at the cell membrane, Cos7 cells were co-transfected with clathrin-dsRed and either dynamin 1-green fluorescent protein (GFP) or dynamin 2-GFP and imaged with TIR fluorescence microscopy. Clathrin puncta were identified and analyzed if they adhered to the following criteria: (i) the clathrin punctum must be diffraction limited, (ii) the clathrin must colocalize with dynamin at some point during the imaging period, (iii) clathrin and dynamin fluorescence must each disappear during the imaging period (the timing of disappearance need not be simultaneous), (iv) while visible, the clathrin must be trackable – i.e. it should not merge with or pass through other regions of clathrin fluorescence and (v) the clathrin must remain visible for at least 20 frames to exclude transient and highly motile structures. We selected puncta which met these criteria in cells transfected with clathrin-dsRed/dynamin1-GFP ($n = 94$) or clathrin-dsRed/dynamin2-GFP ($n = 99$). The puncta were tracked and the average fluorescence intensity was measured over time as described in *Materials and Methods*.

One approach that has been previously used to improve the S/N ratio and to facilitate aggregation of data from many individual puncta is to average fluorescence intensity traces after alignment to a temporal fiducial mark. In previous work, the traces have been aligned to the peak fluorescence of dynamin allowing characterization of the time course of disappearance of clathrin and dynamin (5,6).

Our selection criteria did not required clathrin and dynamin fluorescence to decrease simultaneously. Therefore, there were two separate events common to every trace to which the data could be aligned: the initiation of departure of clathrin or the initiation of departure of dynamin. Average curves for the same 99 puncta are shown in Figure 1A (aligned to initiation of dynamin 2 departure) and Figure 1B (aligned to initiation of clathrin departure).

The point to which the individual traces are aligned had a dramatic effect on the features of the average fluorescence plot. When aligned to the initiation of dynamin departure, there is a clear increase in dynamin fluorescence (a dynamin 'peak') prior to its disappearance (Figures 1A and S1A). This is in contrast to when aligned to the initiation of clathrin departure there is no peak of dynamin 2 and a broadened peak of dynamin 1 (Figures 1B and S1B). Comparison of the averages with individual traces (Figures 1C–F and S1C–F) shows that averaging can be misleading: the average trace is not representative of most of the individual traces. Some individual traces have a peak of dynamin, whereas others do not. Individual traces have differences in the timing between clathrin and dynamin disappearances that explains why the event chosen for alignment affects the result of averaging.
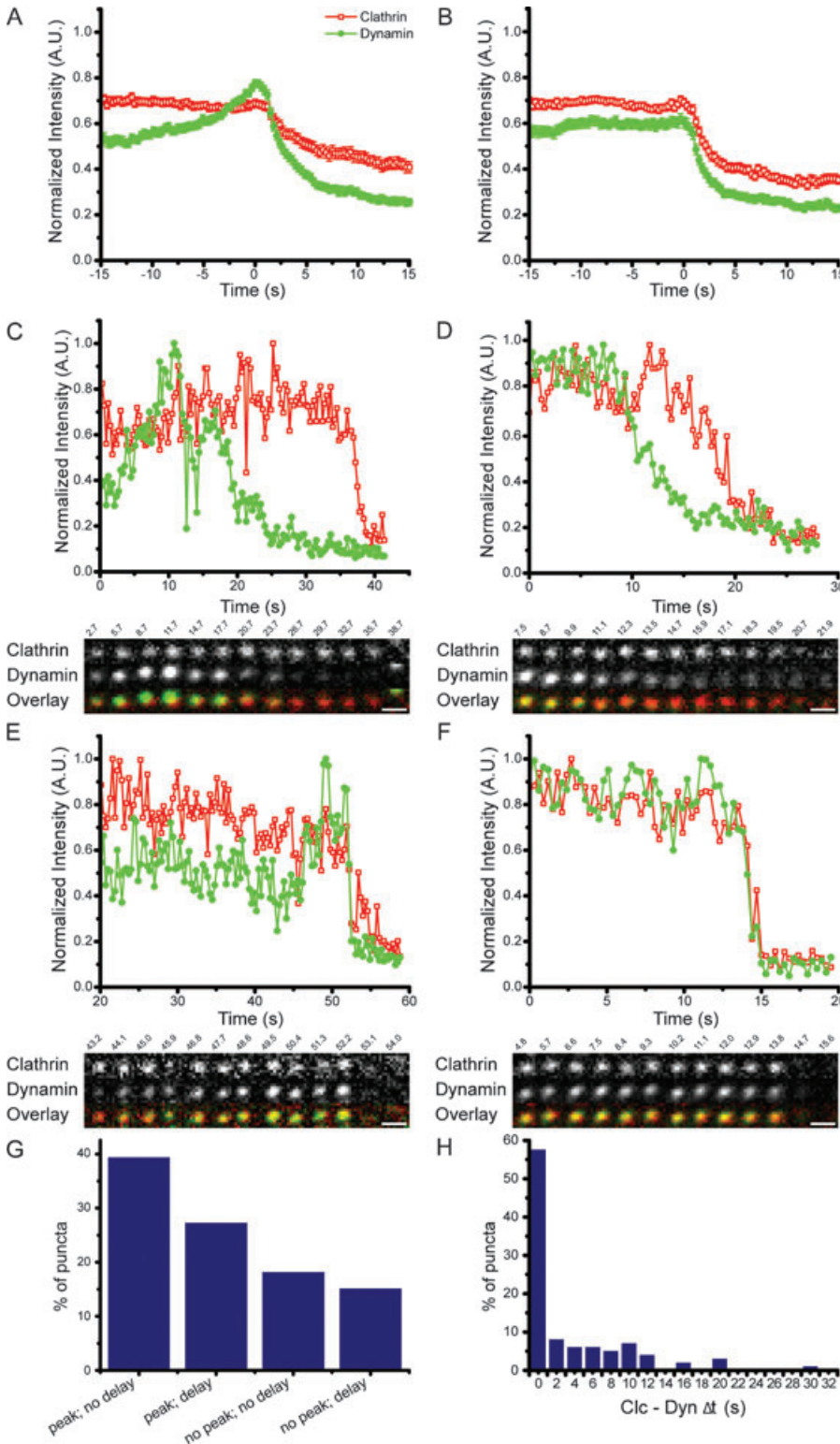
Figure 1: Relative dynamics of clathrin and dynamin 2. Cos7 cells were transfected and imaged with dual color TIR microscopy. Normalized fluorescence intensity is plotted as a function of time for clathrin-dsRed (red, open squares) and dynamin 2-GFP (green, filled circles). A) Average of individual traces aligned to the initiation of dynamin decline ($t = 0$). B) Average of individual traces aligned to the initiation of clathrin decline ($t = 0$). C) Example of an individual punctum with a dynamin peak and the initiation dynamin departure before clathrin. D) Example of an individual punctum without a dynamin peak and the initiation of dynamin departure before clathrin. E) Example of an individual punctum with a dynamin peak and simultaneous initiation of departure of clathrin and dynamin. F) Example of an individual punctum without a dynamin peak and simultaneous initiation of departure of dynamin and clathrin. G) Percentage of puncta exhibiting each type of behavior. H) Histogram of the time between clathrin and dynamin initiation of departure from the evanescent field. Scale bars = 1 μm.

Clathrin and dynamin in individual puncta

Averaging over the entire population of puncta produces variable results depending on how the individual traces are aligned. For these data, averaging is therefore not ideal due to the variability in individual behaviors; one way to illustrate the range of behaviors present is to categorize the data based on patterns of clathrin and dynamin. We divided the spectrum of behavior into four main categories as an aid to visualization (Figure 1G): (i) a delay between the initiation of clathrin and dynamin

departure, with a peak of dynamin fluorescence prior to its departure (Figure 1C), (ii) a delay between the initiation of clathrin and dynamin departure with no peak of dynamin fluorescence (Figure 1D), (iii) simultaneous initiation of clathrin and dynamin departure, with a peak of dynamin fluorescence prior to disappearance (Figure 1E) and (iv) simultaneous initiation of clathrin and dynamin departure with no peak of dynamin fluorescence (Figure 1F). Simultaneous departure was defined as the initiation of clathrin and dynamin departures occurring within 2 seconds of each other. These groups do not necessarily correspond to a particular biological parameter but are useful in highlighting the spectrum of clathrin and dynamin dynamics at the plasma membrane.

For both dynamin 1 and dynamin 2, there were several puncta that did not fit within any of these four categories and were excluded from this analysis. Some puncta had two peaks of dynamin, and in others there was a peak and then the return of dynamin fluorescence to the steady state before the initiation of departure (Figure S2).

There was variability in the times between the initiation of clathrin and dynamin departure. For dynamin 2, in 61% of the events, the initiation of clathrin and dynamin departure was simultaneous. In 39% of the events, there was a delay between the initiation of departure of dynamin and clathrin. For dynamin 1, similar behaviors were observed: in 50% of puncta the initiation of clathrin and dynamin departure was simultaneous and 50% of puncta had a delay between dynamin 1 and clathrin departure. For dynamin 2, we observed delays between the initiation of dynamin departure and the initiation of clathrin departure of up to 30.3 seconds. For dynamin 1, we observed delays of up to 25.5 seconds (Figure 1H). The onset of clathrin disappearance prior to the onset of dynamin decreasing was rarely observed, and dynamin was never present on the membrane after the total disappearance of clathrin.

Diversity in dynamin dynamics

Dynamin 1 expression is limited to neurons and neuroendocrine cells, whereas dynamin 2 is expressed in most cell types. Biochemical differences between dynamin 1 and dynamin 2 have been reported (18), as well as slight differences in their dynamics in live cells (19). In addition to the variability observed between clathrin and dynamin, there was diversity in the dynamic behavior of dynamin. It has been previously reported that there is a transient increase of dynamin fluorescence just prior to its disappearance (5,6). This increase has been termed a peak. In this article, we defined a peak as a 17% increase in intensity over 2.3 seconds (seven time points) of the normalized, averaged signal.

There was a spectrum of dynamin behaviors in the individual puncta. Peaks were observed in 72% of the dynamin 1 puncta and 67% of the dynamin 2 puncta (Figures 1C,E and S1C,E). In 27% of the dynamin 1 and 33% of the dynamin 2 puncta, the level of dynamin fluorescence was constant until it irreversibly declined (Figures 1D,F and S1D,F). The presence or absence of a peak was not correlated with whether or not there was a delay between the initiations of dynamin and clathrin departure.

There are two possible explanations for a peak in dynamin fluorescence: (i) dynamin already present on an invaginated pit is redistributed to the neck and (ii) dynamin is recruited from the bulk solution. Redistribution or recruitment would both lead to an increase in dynamin-GFP fluorescence. Redistribution involves movement of molecules closer to the origin of the evanescent field leading to more efficient excitation and a stronger fluorescent signal; recruitment involves increasing the total number of molecules present.

To differentiate between these possibilities, dynamin 2-GFP and clathrin-dsRed were imaged with alternating epi-fluorescence and TIR excitation. Epi illumination excites all the fluorophores present, whereas in TIR the excitation field decays exponentially from the coverslip with a constant of ~100 nm. If there is a redistribution of dynamin on the vesicle toward its neck, the fluorescence in epi will remain constant while the fluorescence in TIR will increase. If there is recruitment of dynamin, the fluorescence will increase in both TIR and epi. Clathrin- and dynamin-positive puncta with a transient increase in dynamin2-GFP fluorescence in TIR were selected. For all the puncta examined ($n = 59$), there was a concurrent fluorescence increase in both TIR and epi (Figure S3). Therefore, we conclude that the transient increase in fluorescence is the result of dynamin recruitment to the vesicle.

Assay for productive endocytosis

As described above, there is a range of dynamin and clathrin dynamics. To evaluate the relevance of the different dynamics, it is important to establish criteria to identify productive endocytic events. The loss of clathrin fluorescence has often been interpreted as an endocytic event. However, there are number of possible explanations for the loss of clathrin fluorescence: movement of a coated vesicle out of the evanescent field, uncoating of clathrin from the vesicle within the evanescent field or disassembly of a clathrin patch at the cell surface with no endocytic event (an abortive clathrin-coated pit). In the absence of additional information, the cause of the decline in clathrin fluorescence cannot be identified.

One assay that we utilized to identify productive endocytosis was to image fluorescently tagged cargo with alternating epi-TIR. Epi-TIR has been previously used to image clathrin leaving the evanescent field (5,16,17). However, imaging only clathrin cannot distinguish between vesicles uncoating within the evanescent field and abortive pits. In contrast, fluorescently tagged transmembrane cargo cannot dissociate from a formed vesicle and will give a signal in epi as long as the vesicle is present in the focal plane. The cargo utilized was EGF receptor (EGFR), which

has been shown to retain functionality when tagged with GFP (EGFR-GFP) (20).

Imaging cargo with epi-TIR allows identification of the internalized vesicles. TIR provides the axial discrimination to identify plasma membrane associated puncta while epi allows vesicles to be tracked as they leave the evanescent field. It is not possible to determine the origin of vesicles using epi alone, while using only TIR does not distinguish between departure of a vesicle from the membrane and disassembly of clathrin. Puncta visible in TIR were considered to be at the plasma membrane; these puncta are also visible in epi. A punctum that left the evanescent field while remaining in epi was interpreted as an internalized vesicle arising from a productive endocytic event.

This assay identifies vesicle internalization from the plasma membrane directly, rather than using disappearance of clathrin fluorescence as a proxy for productive endocytosis. This assay identifies puncta, which have undergone endocytosis by determining the time at which these vesicles depart the plasma membrane. However, it does not identify scission of the vesicle.

Clathrin uncoating dynamics are variable

Cos7 cells were transfected with clathrin-dsRed and EGFR-GFP and imaged with epi-TIR. Puncta were selected for further analysis based on the following criteria: (i) clathrin colocalizes with EGFR at some point, (ii) the EGFR signal disappeared from the TIR channel over the course of imaging and (iii) puncta could be unambiguously tracked up to the point to disappearance of EGFR from the evanescent field.

We analyzed 80 puncta, and of these, 88.75% were unambiguously identified as endocytic events by loss of EGFR fluorescence in TIR while maintaining EGFR fluorescence in epi (Figure 2). A spectrum of behaviors was observed which can be categorized into four groups. In the first group, the initiation of clathrin and EGFR fluorescence departure from TIR was simultaneous (within 2 seconds of each other), while both clathrin and EGFR continued to be visible in epi (35%) (Figure 2A). This was interpreted as a vesicle leaving the evanescent field prior to clathrin uncoating. Within the imaging time, almost half of the vesicles in this population lost clathrin fluorescence in epi before EGFR fluorescence, indicating that uncoating occurred outside the evanescent field.

In the second group, the initiation of clathrin departure from both epi and TIR occurred simultaneously. After clathrin loss, the EGFR signal departed TIR and remained in epi (31.25%) (Figure 2B). This represents a vesicle losing its clathrin coat close to the plasma membrane, before the vesicle moves into the cell.

In the third group, the initiation of departure of clathrin from TIR and epi occurred simultaneously with disappearance of EGFR from TIR. EGFR fluorescence remained in epi (22.5%) (Figure 2C). This indicates the vesicle uncoating as it moves away from the plasma membrane into the cell.

In the fourth group, the initiation of departure was simultaneous for clathrin and EGFR, in both epi and TIR (11.25%). For these puncta, it could not be resolved if they were endocytic with an inward movement faster than the frame rate of our camera, or if disassembly of the endocytic site was occurring (Figure 2D).

Vesicle scission

The difference in timing between the initiation of clathrin and dynamin disappearance and the variety in clathrin uncoating suggest that the vesicles linger proximal to the plasma membrane after they have separated from it. While EGFR disappearance from TIR before epi is a good marker for productive endocytosis, it does not indicate when the vesicle separates from the plasma membrane.

Scission was determined by measuring when the lumen of a nascent endocytic vesicle becomes inaccessible to extracellular protons (14).This assay uses pHlourin (pHl), a pH-sensitive GFP for which the fluorescence is high at pH 8 and low at pH 5.5 (21). Transferrin receptor (TfR), which is constitutively endocytosed, was tagged with pHl on its external domain (TfR-pHl). Cos7 cells were transfected with TfR-pHl and imaged while the pH of the external media alternated between 5.5 and 8.0. TfR-pHl which is accessible to the external media is affected by the changes in pH and cycle between low and high fluorescence. However, after scission from the plasma membrane, the internal pH of the vesicle will reflect the pH of the media at the time of scission and will not be affected by changes in external pH. Insensitivity to external pH is interpreted as scission, although this could also be due to a hemi-scission event. Scission is detectable only when the solution inside the vesicle has a high pH and the pHl is fluorescent; scission events which occur at low pH are undetectable in this assay (5).

Cells were transfected with TfR-pHl and clathrin-dsRed. We identified 90 puncta where TfR-pHl colocalized with clathrin-dsRed and underwent scission (Figure 3). Of these, 10 appeared to regain pH sensitivity and were not analyzed further.

The intensity of a diffraction-limited spot of TfR is measured over time by calculating the average intensity of a region of interest (ROI) encompassing the punctum. The ROI will contain both the forming vesicle and diffuse TfR on the surrounding membrane. After scission, the intensity of the vesicle will be insensitive to the surrounding pH, while the plasma membrane associated receptor fluorescence will continue to fluctuate. There will therefore always be some residual cycling in the average intensity measured. However, we can clearly identify scission as the point at which the vesicle becomes insensitive to the external pH and only exhibits a low level
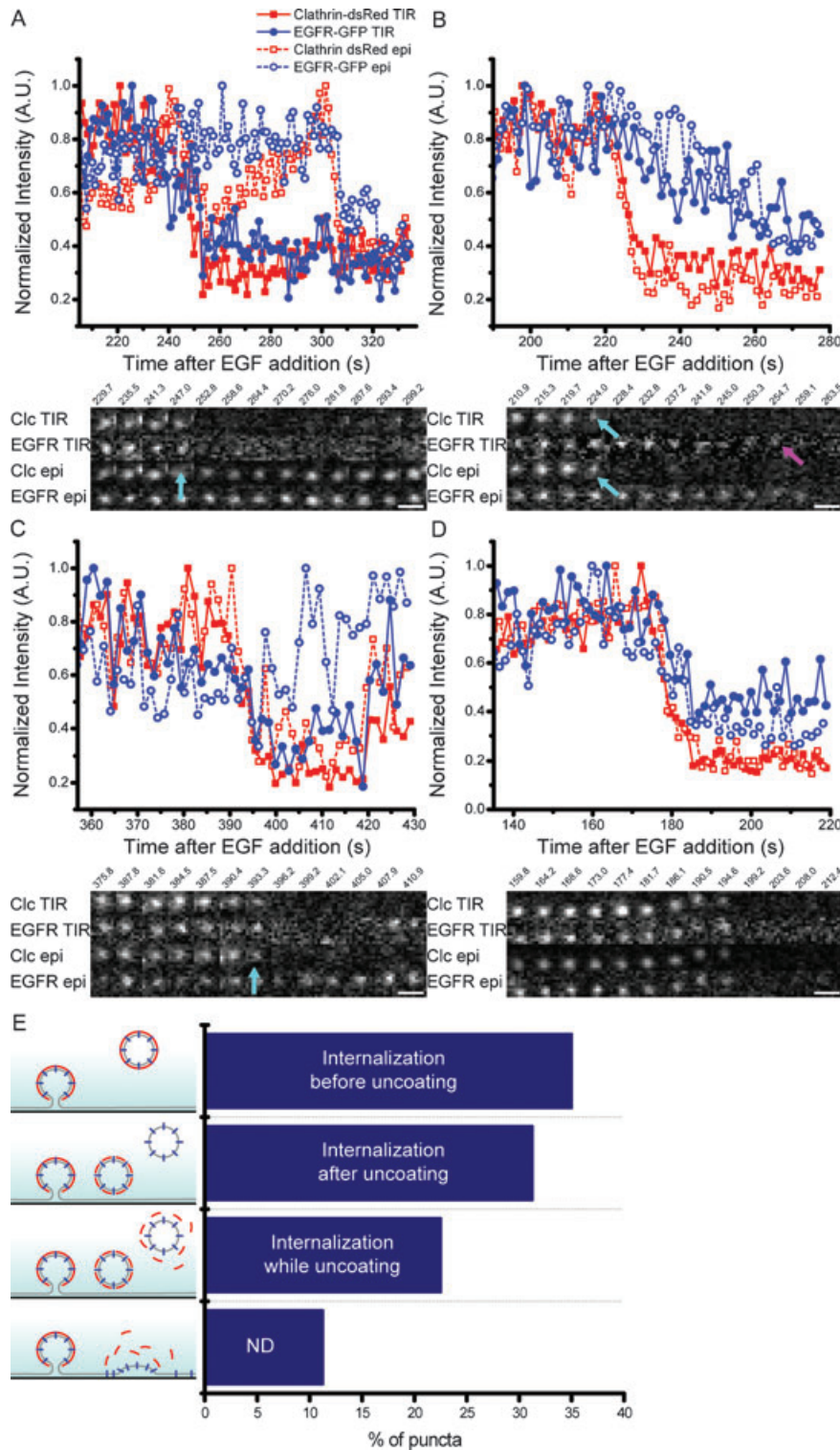
Figure 2: Identification of internalizing puncta. Cos7 cells were transfected and imaged with dual color epi-TIR microscopy. Normalized fluorescence intensity is plotted as a function of time EGFR-GFP (blue, circles), clathrin-dsRed (red, squares), TIR (solid lines and filled markers) and epi (dashed lines and open markers). A) Example of an individual punctum where initiation of EGFR and clathrin fluorescence decline in TIR is simultaneous (cyan arrow), and prior to loss of EGFR and clathrin fluorescence in epi. B) Example of an individual punctum where initiation of clathrin fluorescence decline in TIR and epi is prior to the initiation of EGFR fluorescence decline in TIR. Loss of clathrin fluorescence is indicated by the cyan arrows and loss of EGFR fluorescence in TIR is indicated by the magenta arrow. C) Example of an individual punctum where the initiation of clathrin TIR, clathrin epi and EGFR TIR fluorescence decline is simultaneous, while EGFR remains visible in epi. The loss of clathrin epi, clathrin TIR and EGFR TIR is indicated by the cyan arrow. D) Example of an individual punctum in which all four signals begin to decline simultaneously. E) Percentage of puncta displaying each of the four types of behavior described in (A), (B), (C) and (D). Scale bars = 1 μm.

cycling due to residual TfR at the plasma membrane (Figure S4).

Once again a spectrum of behaviors was seen for the timing of scission relative to the initiation of clathrin departure. In 22.5% of the puncta, the initiation of clathrin fluorescence decline was at, or within 5 seconds of, scission and was identified as simultaneous (Figure 3A). In 50% of puncta, there was a delay between scission and the initiation of clathrin departure (Figure 3B). The maximum time between scission and the initiation of clathrin departure was 150.7 seconds. In 27.5% of puncta,
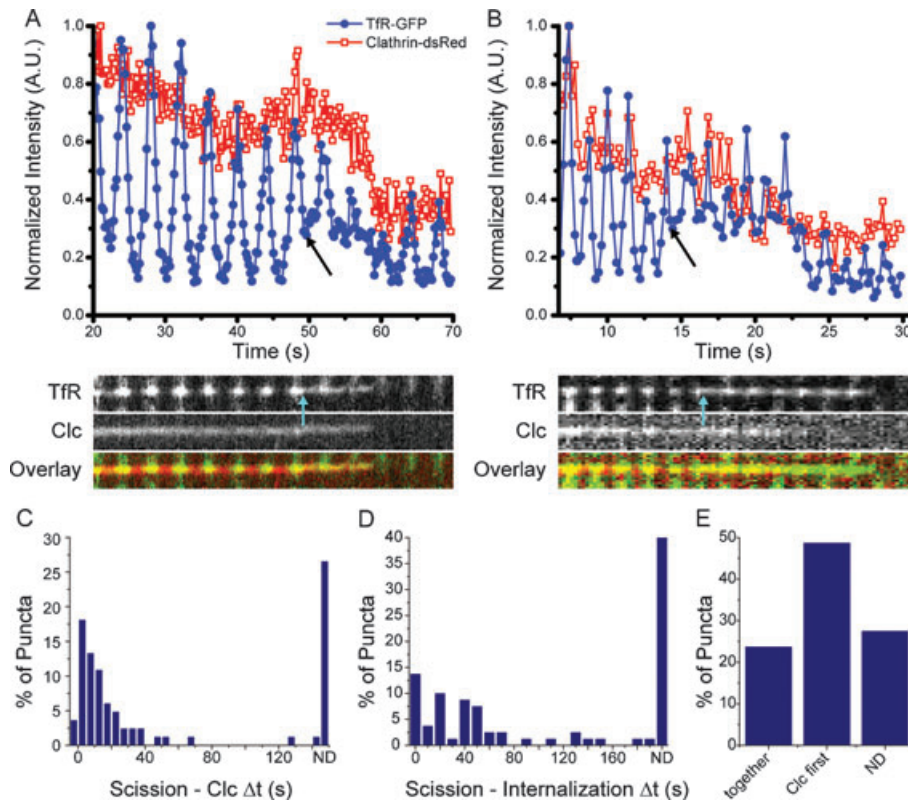
Figure 3: Vesicle scission and clathrin dynamics. Intensity is plotted as a function of time for TfR-pHl (blue, filled circles) and clathrin-dsRed (red, open squares) and a kymograph [overlay: clathrin (red) and TfR (green)]. A) An example of scission (plot, black arrow and kymograph, cyan arrow) followed by simultaneous initiation of departure of TfR and clathrin. B) An example of scission (plot, black arrow and kymograph, cyan arrow) followed by initiation of departure of clathrin fluorescence prior to that of TfR fluorescence. C) Histogram of the time between scission and the initiation of clathrin fluorescence decline. D) Histogram of the time between vesicle scission and initiation of departure of TfR from the evanescent field (internalization). E) Percentage of puncta in which initiation of clathrin and TfR departure is simultaneous, initiation of clathrin departure is first or both fluorophores are still present at the end of the imaging period and the dynamics cannot be determined (ND).

neither the TfR nor the clathrin fluorescence intensity had declined by the end of the imaging period. These puncta are scissioned vesicles, which are still present in the evanescent field (Figure 3C).

Disappearance of a punctum from the cell surface does not therefore represent scission but rather movement of the vesicle out of the evanescent field. In 24% of the puncta, the initiation of clathrin and TfR fluorescence decline was simultaneous (Figure 3A,D,E). These events are interpreted as the vesicle leaving the evanescent field before clathrin uncoating has taken place. In 49% of the puncta, clathrin uncoated from the nascent vesicle before it left the evanescent field, i.e. following clathrin departure a TfR-pHl signal remained (Figure 3B,D,E). In the remaining 28% of puncta, clathrin and TfR were still present at the end of the imaging period and their relative dynamics could not be determined.

Thus, the initiation of clathrin departure from the evanescent field is not a good marker for either scission of the vesicle from the plasma membrane or the

time a vesicle leaves the proximity of the membrane (Figure 3D,E). Uncoating of clathrin, movement away from the surface and scission are three separate processes that do not appear to be temporally correlated.

Dynamin is known to be involved in scission but may leave the neck shortly before, shortly after, or as the vesicle separates from the plasma membrane (22–25). Dynamin departure from the evanescent field may, or may not, be a good marker for the biophysical process of scission. We next investigated the correlation of dynamin dynamics with scission.

Cells were transfected with TfR-pHl and dynamin 2-mCherry. We selected 65 puncta in which TfR-pHl and dynamin 2-mCherry colocalized and underwent scission. However, of these, four appeared to regain pH sensitivity and were not included in the analysis. Scission occurred both in the presence and the absence of a transient dynamin peak. In 21% of puncta there was a dynamin peak, while in 79% of puncta there was not (Figure 4A–D). Therefore, a dynamin peak is not necessary for vesicle
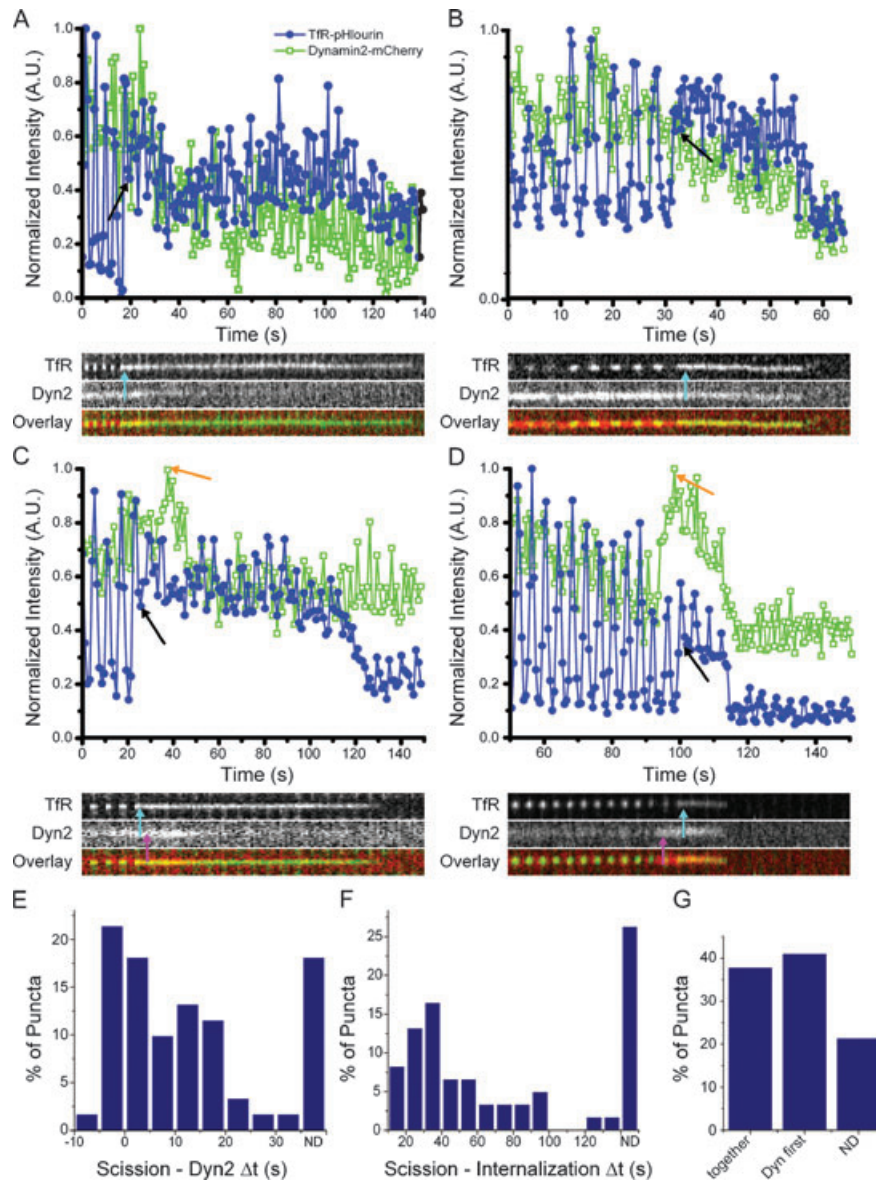
Figure 4: Vesicle scission and dynamin dynamics. Intensity as a function of time for TfR-pHI (blue, filled circles) and dynamin 2-mCherry (green, open squares) and kymograph [overlay: dynamin (red) and TfR (green)]. A) An example of scission (plot, black arrow and kymograph, cyan arrow) followed by initiation of decline of dynamin fluorescence without a peak, and prior to initiation of decline of TfR fluorescence from the evanescent field. B) An example of scission (plot, black arrow and kymograph, cyan arrow) followed by simultaneous initiation of decline of dynamin and TfR fluorescence. There is no dynamin peak. C) An example of scission (plot, black arrow and kymograph, cyan arrow) followed by initiation of decline of dynamin fluorescence prior to that of TfR fluorescence. There is a peak of dynamin fluorescence (plot, orange arrow and kymograph, magenta arrow). D) An example of scission (plot, black arrow and kymograph, cyan arrow) followed by simultaneous initiation of decline of dynamin and TfR fluorescence. There is a peak of dynamin fluorescence (plot, orange arrow and kymograph, magenta arrow). E) Histogram of the time between vesicle scission and initiation of decline of dynamin fluorescence. F) Histogram of the time between vesicle scission and the initiation of TfR fluorescence decline (internalization). G) Percentage of puncta in which initiation of clathrin and TfR departure is simultaneous, initiation of clathrin decline begins first or both fluorophores are still present at the end of the imaging period and the dynamics cannot be determined (ND).

scission. When there was a dynamin peak, the apex of the peak occurred within 13 seconds of scission. Although the apex of the peak and the scission event were not always coincident, the scission event occurred during the period of increased dynamin fluorescence (13/13).

Surprisingly, the initiation of dynamin departure from the nascent vesicle was variable with respect to scission. In 14 cases, the initiation of dynamin fluorescence decline was just prior to scission (<5 seconds), although dynamin was still present on the vesicle at the time of scission.

In all other cases, the initiation of dynamin departure was simultaneous with or after scission, with delays of up to 31 seconds after scission (Figure 4E).

The time for which the TfR-pHl remained in the evanescent field after scission varied from 5.4 to 130.3 seconds. This confirms that the nascent vesicle does not have to be immediately internalized and can remain proximal to the plasma membrane for some time after scission (Figure 4F,G). In 26% of cases, the TfR-pHl fluorescence was still present at the end of the imaging period and the lifetime in the evanescent field after scission could not be determined.

The initiation of dynamin decline was variable with respect to vesicle internalization. In 38% of events, the initiation of dynamin and TfR fluorescence decline was simultaneous indicating that dynamin can remain on the vesicle even as it leaves the evanescent field (Figure 4B,D). In 41% of events, the initiation of dynamin departure was before the initiation of TfR fluorescence departure. This indicates dynamin dissociation from the vesicle after scission but before movement away from the membrane (Figure 4A,C). In the remaining 21% of puncta, both the dynamin and TfR signals were present in the evanescent field at the end of the imaging period.

Discussion

The internalization of cargo via endocytosis involves the coordination of many factors including extracellular cargo, transmembrane receptors, lipids, cytosolic adaptor and coat proteins, and the GTPase dynamin. Understanding the roles of different molecules in this process requires a full picture of the dynamics of all these players relative to physical and membrane events. In this study, we implemented and established assays for physical events in endocytosis – specifically, scission of the vesicle from the plasma membrane and movement of the vesicle into

the cell. We characterized the dynamics of clathrin and dynamin on individual vesicles relative to these physical events. Importantly, both assays used fluorescently tagged membrane-bound cargo, which cannot dissociate from the vesicle.

The data presented here show variable dynamics of dynamin and clathrin relative to each other and relative to the physical events of scission and movement away from the surface. Clathrin and dynamin can dissociate from the vesicle at the same time, or dynamin can dissociate first. However, we never observed measurable amounts of dynamin remaining on the membrane following loss of the clathrin coat. Dynamin departure can begin prior to, simultaneously with, or after scission. The initiation of clathrin departure can occur at variable times after scission. Clathrin and dynamin dissociation from the nascent vesicle can happen either before or after movement away from the plasma membrane (Figure 5).

Our data show that the dynamin peak is due to recruitment from the bulk solution rather than rearrangement of dynamin on the vesicle. It is not clear from these data whether the recruited dynamin is targeted specifically to the neck. A dynamin peak is not required for scission and a transient increase of dynamin is therefore not a good criterion for the selection of productive endocytic events. These peaks may have mechanistic relevance, but the actual mechanism of dynamin action cannot be determined from these data. A model whereby dynamin pushes the nascent vesicle away into the cell while remaining behind on the plasma membrane is not consistent with the observation that the initiation of clathrin fluorescence loss is never before the initiation of dynamin fluorescence loss.

A number of biological and technical factors (discussed below) may contribute to the diversity of behaviors observed. However, the relationship between these factors and the clathrin and dynamin dynamics we
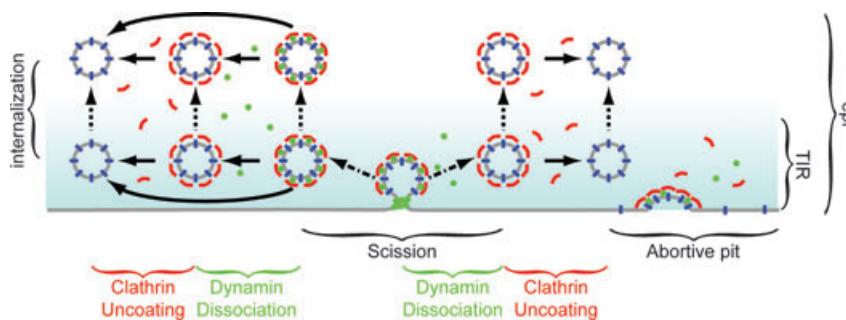

Figure 5: Model for vesicle scission, uncoating and internalization. This model depicts the dynamics of cargo (blue), clathrin (red), and dynamin (green) in clathrin-mediated endocytosis. The evanescent field is shown in cyan. The physical events measured in endocytosis are indicated by arrows: scission (dash-dot arrows), uncoating (solid arrows) and internalization (dotted arrows). Dynamin can leave a vesicle concurrently with scission, prior to internalization or after internalization. Clathrin uncoating occurs after scission but either before or after internalization. If cargo and clathrin or dynamin are present and no physical event is measured, this could represent an abortive pit.

observe is unclear. It is likely that the spectrum of behaviors observed is a result of multiple factors and does not reflect discrete populations with differing activities.

Within a population, clathrin disappearance from the evanescent field could be due to uncoating of a nascent vesicle, movement of a vesicle out of the evanescent field or an abortive pit. Variation in the time at which clathrin fluorescence remains after scission could be due to stochasticity in uncoating. Alternatively, it is possible that uncoating behaviors could depend on the composition of cargo within the vesicle or the ultimate destination of the vesicle within the cell (26,27).

These data show that the time a vesicle remains at or near the plasma membrane after scission before moving into the cell is variable. This may be because a vesicle engages with cytoskeletal machinery for transport to its destination in a stochastic manner. It has been reported that F-actin is not obligatory for clathrin-mediated endocytosis in mammalian systems (28). However, studies in which actin and clathrin were imaged together have shown bursts of actin fluorescence which colocalize with clathrin-coated pits (5), although these were only reported in a subset (80%) of the clathrin-coated pits. Imaging of cortactin has shown it localizing to only 36% of membrane scission sites. (14). Tracking the movements of clathrin-coated pits and vesicles in the evanescent field reveals that for the majority of puncta, there is initially very little lateral movement. This would be expected for a forming clathrin-coated pit, which is tethered to its position on the cell membrane. Interestingly, two subsets of vesicles with increased lateral mobility before leaving the evanescent field were noted. The first subset began moving in a random manner, which might be expected for a scissioned vesicle that is diffusing. The second subset exhibited fast, directed motion which may be attributable to movement on the cytoskeleton. This disparity could explain the variation in the times nascent vesicles are present at the surface before internalization.

There are biological factors that could influence vesicle behavior. The make up of the cargo in the vesicle may affect vesicle trafficking. For example, overexpression of the TfR has been shown to increase the percentage of longer lived clathrin-coated pits (9), and it has been suggested that cargo capture stabilizes clathrin pits as they are forming (8). Not all vesicles will contain the same cargo; it has been shown that G- protein-coupled receptors are recruited to only a subset of vesicles (11). It is possible that the cargo present in a nascent vesicle could influence the dynamics of other endocytic proteins (29). In the future, it will be interesting to compare clathrin and dynamin dynamics with different cargo molecules. There is also evidence that the dynamics of clathrin-mediated endocytosis can depend on cell type: variation in the lifetimes and dynamics of clathrin-coated pits has been shown between HeLa and Bsc1 cells (9).

Other factors can affect the data and the conclusions drawn from this type of experiment. In the literature, live cell studies have used a variety of imaging modalities; including TIR, epi and confocal microscopy. Even within TIR imaging studies, the measured residence times at the plasma membrane will be expected to differ as a function of the evanescent field depth. Other factors that will influence the data include the tagged proteins, the fluorescent label, temperature, the sensitivity of the camera and the imaging rate. Differences in selection criteria will lead to identification of different subpopulations of puncta.

When selecting puncta for analysis, diffraction-limited clathrin spots were identified and assumed to represent individual clathrin-coated pits. As has been seen in electron microscopy, clathrin exists on the basolateral surface of cells in invaginations and flat lattices that are sometimes contiguous or in close proximity (30). Features smaller than the resolution limit of the light microscope, approximately 250 nm, cannot be resolved. It is possible that some diffraction-limited spots identified contain more than one clathrin structure. Recent advances in super-resolution microscopy, specifically structured illumination TIRF, could be very helpful in addressing this heterogeneity (31).

In this study, as with others, not every fluorescent puncta present in the evanescent field was analyzed. Whether puncta for analysis are selected manually or computationally, there is always an element of bias introduced by the selection criteria. The criteria used to identify endocytic events relied upon physical markers of this process. However, while we believe every spot analyzed in these assays was a genuine endocytic event, every endocytic event was not analyzed. Below we discuss details of the assays used to identify the physical events in endocytosis.

Imaging cargo with epi-TIR allowed identification of vesicles, which unambiguously moved into the cell. The cargo molecule, GFP-tagged EGFR, has several properties which make it a useful tool in this assay. Following incubation in serum-free media, EGFR is diffused at the plasma membrane, resulting in a low internal background fluorescence within the cell. On the addition of EGF, EGFR clusters in preformed clathrin puncta and endocytosis begins within 6–10 min (32); thus, the timing of EGFR endocytosis can be controlled. The initial low internal background facilitates differentiation between vesicles pinching off from and leaving the plasma membrane and previously internalized vesicles.

Scission of the vesicle from the plasma membrane was assayed by TfR-pHl sensitivity to external pH changes. One caveat of this assay is that it does not distinguish between hemi-fission and full fission of the vesicle from the membrane, a specific step invoked in some models of dynamin mechanism. (22,33). A small fraction of puncta

lost and later regained sensitivity to the external pH (10/90 for clathrin/TfR and 4/65 for dynamin/TfR). These potentially represent hemi-fission events which reopen to the external medium rather than proceeding to full fission. Another possibility is that these puncta represent to multiple pits, which are closer together than the diffraction limit, only one of which underwent scission and internalization.

For technical reasons the scission assay was conducted at room temperature, approximately at 25°C rather than the physiological 37°C. It is expected that the lower temperature could slow cellular dynamics, including those involved in endocytosis, leading to longer residence times at the membrane after scission and prior to internalization. The lower temperature could also alter the transition dynamics to full scission from a hemi-scission intermediate, which would change residence time at the membrane.

While interpreting the scission assay data, there are several points worth considering. First, there are several factors that could affect the fluorescence intensity: (i) pHl photobleaching, (ii) pH at the time of image acquisition (the pH is constantly changing and image acquisition is not precisely coordinated with the maximum pH of 8.5, which contributes to variations in the maximum fluorescence intensity recorded, (iii) fluctuation in the number of fluorophores, their position and orientation, (iv) changes in focus caused by perfusion and (v) background fluorescence including other nearby fluorescent puncta. Second, in some of the puncta following scission there is some residual cycling of fluorescence intensity. Crucially, the minimum value of this cycling never returns to the background level, as the receptors in the scissioned vesicle remain inaccessible to pH changes and therefore fluorescent. There are several possible explanations for this residual cycling. One is the contribution of background intensity fluctuations to the measured average fluorescence from an ROI. This could be from residual receptors on the surface that are not internalized within the area visualized or the proximity of another nascent endocytic pit. The relative contribution of background will be greater if the scission occurred at a lower pH, when the endocytic vesicle was at a low fluorescence intensity. A second factor, which could contribute, is a fluctuation in focus. The focus is slightly affected by the perfusion of solution, and the coverslip may move as the solution is switched, causing the intensity of a vesicle to fluctuate slightly in a periodic manner. Finally, it is also possible that the neck of the nascent vesicle is constricted enough to offer significant resistance to proton flow, but has not undergone scission.

Here, we implement and show the importance of assays for vesicle internalization and scission. This approach can be extended to investigate other physical events in endocytosis such as the invagination of the flat membrane to form a clathrin-coated pit (13). These tools for identifying physical and membrane changes and positive endocytic events can be used to examine other proteins such as adaptors (e.g. AP2) or BAR domain proteins which are implicated in stabilizing membrane curvature. Experiments which combine the investigation of protein dynamics with identification of biophysical events common to all vesicles have the potential to reveal relevant similarities and meaningful differences in biological processes.

Materials and Methods

Plasmids
Dynamin
Monomeric enhanced GFP (mEGFP) was constructed from EGFP-N1 (Clontech Laboratories, Inc.) using site-directed mutagenesis (34). Dynamin 1aa from *Rattus norvegicus* tagged with EGFP (from Pietro de Camilli, Yale School of Medicine) and dynamin 2aa from *R. norvegicus* tagged with EGFP (from Mark McNiven, Mayo Clinic) were digested with AgeI and BsrGI and ligated to mEGFP or mCherry-N1(Clontech) digested with AgeI and BsrGI to create the tagged dynamin constructs: dynamin 1-mEGFP, dynamin 2-mEGFP (referred to as dynamin 1-GFP and dynamin 2-GFP), dynamin 1-mCherry and dynamin 2-mCherry.

Epidermal growth factor receptor-green fluorescent protein
Rat EGFR tagged with EGFP (EGFR-GFP) was a gift from Alexander Sorkin (University of Colorado Health Sciences Center).

Transferrin receptor-pHlourin
pHl was amplified by polymerase chain reaction from Gag-pHl (35) using the following primers: forward primer, GCGCACCGGTCGCCACC ATGAGTAAAGGAGAACTTTTC (introducing an AgeI site) and reverse primer, GCGCTCTAGATTAGTTATTTGTATAGTTCATCCATGCC (introducing an XbaI site). pHl was inserted into TfR-EGFP plasmid (from Alex Benmerah) as a replacement for GFP at the AgeI and XbaI sites.

Clathrin-dsRed
Rat clathrin light chain A was tagged with dsRed (clathrin-dsRed) (from Tomas Kirchhausen, Harvard Medical School).

Cell culture
Cos7 cells were grown in DMEM (Invitrogen) supplemented with 10% FBS and 5% Pen/Strep with 5% CO_2 at 37°C. Cells were plated onto sterile glass coverslips (VWR) and transfected with Lipofectamine 2000 (Invitrogen) according to the manufacturer's instructions. In the perfusion experiments, cells were plated into tissue culture treated μ-slide l 0.6 Luer chambers (Ibidi) and transfected with Fugene6 (Roche) according to the manufacturer's instructions. Cells were imaged 12–48 h after transfection.

EGFR internalization
The protocol used for observing internalization of individual EGFR puncta via clathrin-mediated endocytosis was as previously described (32). In summary, cells were incubated in serum-free media for 15 min. An individual cell was identified and 100 ng/mL of EGF was added to the dish. Images were acquired once every 30 seconds until EGFR-GFP puncta were observed whereupon the imaging rate was increased to every 300 milliseconds. Experiments were carried out at 37°C.

TfR-pHl vesicle scission
Cells were plated in ibidi μ-slide chambers. Fluid flow was controlled with a pinch valve perfusion system (AutoMate Scientific). Phosphate buffers

with a pH of 5.5 and 8.5 were alternately perfused (every 2 seconds) into the imaging chamber. A 7.2 pH buffer was perfused onto the cells when data were not being acquired. Experiments were conducted at room temperature (~25°C).

Microscopy

Two similar microscopes were used in these experiments. The first microscope was an Olympus IX70 equipped with a prototype TIRF combiner (Olympus) and a 60 × 1.45 NA objective. The laser excitation used in these experiments was 488 nm to excite GFP and dsRed (SpectraPhysics, Newport) and 568 nm to excite mCherry (Melles Griot, CVI Melles Griot). The dichroics used were 488lp (GFP and dsRed) and a 488/568 polychroic (GFP and mCherry). The microscope has an OrcaER charge-coupled device (CCD) camera (Hamamatsu) and images were acquired at 0.09 µm/pixel.

Alternating epi-TIR images were acquired using custom mounted 50/50 prism which allowed illumination either via the back-mounted Xe lamp (epi) or the side-mounted laser TIRF combiner. The excitation sources were controlled via METAMORPH (Molecular Devices). Epi excitation was controlled via a shutter (Uniblitz) and TIR was controlled by an AOTF (Neos Technologies). The epi excitation filter was 470/40.

The second microscope was an Olympus IX70 with a home-built TIRF illuminator. The laser was directed to the objective by a pair of galvanometers and a custom side-facing dichroic mirror. The laser excitation was 488 nm to excite GFP and dsRed (Melles Griot) and 543 nm to excite mCherry (Melles Griot). The dichroics used were a 488lp (GFP and dsRed) and a 488/542 polychroic (GFP and mCherry). The galvanometers were controlled via METAMORPH. Alternating epi-TIR images were acquired by changing the angle of incidence of the laser with the galvanometers. The microscope has an OrcaER CCD camera (Hamamatsu) and images were acquired at 0.09 µm/pixel.

On both microscopes, the fluorescence emission was collected simultaneously and split into two images (green and red) with a Cairn OptosplitIII emission splitter (Cairn Research Limited) with an ET525/50 bandpass filter for GFP emission, an ET632/60 bandpass filter for dsRed and mCherry emission and a 580lp dichroic mirror to split the emission. All dichroics, excitation and emission filters were from Chroma Technologies.

All experiments were conducted at 37°C except for those involving TfR-pHl, which were conducted at room temperature (~25°C).

Image analysis

Red and green fluorescence emission channels were split and aligned using the IMAGEJ PLUGIN CAIRN IMAGE SPLITTER ANALYZER for IMAGEJ (rsbweb.nih.gov/ij). Background was subtracted using the rolling ball background subtract function with a radius of 10 and no smoothing.

Clathrin/dynamin experiments

Cellular subregions were selected. All spots in these regions were identified and circled in the first frame of the clathrin channel. The positions of these spots were transferred to the dynamin channel and the average intensity was calculated for each frame. These data were exported to MATLAB (The MathWorks) where they were displayed graphically for spot selection. Spots were selected for further analysis if a fluorescence signal was present in both channels, the spot disappeared from both channels during the stream and the spot did not merge with or move over other spots during the stream. The spots selected for further analysis were tracked using the IMAGEJ PLUGIN SPOTTRACKER 2D to track the center of each clathrin spot for the duration of its presence. The coordinates of the centroids of all the tracked spots were exported to MATLAB. Circular regions of interest were centered at these coordinates and the average intensity within the ROI was measured in all channels and exported for further analysis. The data

were normalized to the maximum intensity in each channel for each spot. To determine the time of initiation of fluorescence decline, we first applied a rolling average to the data using a seven-frame window. The initiation of departure was determined as the point at which the fluorescence intensity of a particular spot started to decline irreversibly, and assigned to the middle time point from the rolling average. 'Simultaneous' departure was assigned to those traces in which the initiation of the clathrin and dynamin departures occurred within 2 seconds (six frames) of one another. To determine the presence or absence of a peak, the rolling average of the intensity was calculated using a window of seven frames. Dynamin peaks were defined as a rise in dynamin by more than 17% of the normalized, averaged signal over seven frames (2.3 seconds). All averages were made with the normalized (not averaged) data. Fluorescence intensities were exported from MATLAB and were analyzed in MICROSOFT EXCEL.

EGFR/clathrin experiments

Initially, images were acquired every 30 seconds after the addition of EGF. When EGFR was observed clustering into spots, the image acquisition rate was increased to every 300 milliseconds. Cellular subregions were identified, and all spots in the EGFR TIR channel circled. The spot positions were transferred to the EGFR epi and both clathrin channels, and the average intensity of the region for each channel was calculated in each frame. Spots were selected for further analysis if a fluorescence signal was present in all channels, the spot disappeared from both TIR channels during the stream, and if the spot did not merge with or move over other spots during the stream. The spots selected for further analysis were tracked in the EGFR epi channel as described above. The coordinates of the centroids of all the tracked spots were exported to MATLAB. Circular regions of interest were centered at these coordinates and the average intensity within the ROI was measured in all channels. Spots were considered to have been productively endocytic if the EGFR signal remained in the epi channel for more than two frames after it was no longer detectable in the TIR channel. Data were analyzed using the IMAGEJ SPOTTRACKER 2D, MATLAB and MICROSOFT EXCEL as described fully for the clathrin/dynamin experiments.

TfR-pHl experiments

Spots were selected in the TfR channel and the positions of these spots were transferred to either the clathrin of dynamin channels. Spots were analyzed further if the receptor colocalized with the second marker (dynamin-mCherry or clathrin-dsRed) and if the TfR became insensitive to pH changes at some point during the imaging period. The point of scission was identified using the average intensity trace for TfR-pHl as the first frame in which the signal stopped cycling in response to the pH changes. Spots were tracked in the TfR channel. The initiation of departures of clathrin, dynamin and TfR were calculated as described above for the clathrin/dynamin experiments. For the dynamin-mCherry constructs, there was a higher local background and therefore more noise. We therefore modified the criteria used to select peaks: the intensity was averaged over time using a rolling window of 10 frames. Dynamin peaks were calculated as an increase in fluorescence of more than 12% over 20 frames followed by a decrease in fluorescence. Data were analyzed using the IMAGEJ SPOTTRACKER 2D, MATLAB and MICROSOFT EXCEL as described above for the clathrin/dynamin experiments.

Acknowledgments

Supporting Information

Additional Supporting Information may be found in the online version of this article:

Figure S1: Relative dynamics of clathrin and dynamin 1. Cos7 cells were transfected and imaged with dual color TIR microscopy. Individual puncta were selected and normalized fluorescence intensity is plotted as a function of time of clathrin-dsRed (red, open squares) and dynamin 1-GFP (green, filled circles). A) Average of traces aligned to the time of initiation of dynamin departure ($t = 0$). B) Average of traces aligned to the time of initiation of clathrin departure ($t = 0$). C) Example of an individual punctum with a dynamin peak and initiation of dynamin decline before that of clathrin. D) Example of an individual punctum without a dynamin peak and initiation of dynamin decline before clathrin. E) Example of an individual punctum with a dynamin peak and simultaneous initiation of clathrin and dynamin departure. F) Example of an individual punctum without a dynamin peak and simultaneous initiation of dynamin and clathrin decline. G) Percentage of puncta exhibiting each type of behavior. H) Histogram of the time between initiation of clathrin and dynamin departures from the evanescent field. Scale bars = 1 μm.

Figure S2: Uncategorized dynamin 1 dynamics. Cos7 cells were transfected and imaged with dual color TIR microscopy. Individual puncta were selected and normalized fluorescence intensity plotted as a function of time of clathrin-dsRed (red, open squares) and dynamin 1-GFP (green, filled circles). Dynamin 1 peaks are indicated by cyan arrows. A and B) Examples of puncta where there is a peak of dynamin 1 fluorescence followed by a return to the prepeak steady-state level before loss of fluorescence. C and D) Examples of puncta with multiple dynamin 1 peaks.

Figure S3: The dynamin peak is caused by dynamin recruitment from the bulk. Cos7 cells were transfected with dynamin 2-GFP and imaged with epi-TIR microscopy. Normalized intensity is plotted as a function of time for TIR (red with open squares) and epi (green with closed circles). A B and C) Individual examples of puncta where there was a dynamin peak.

Figure S4: Effect of membrane TfR cycling on background. One ROI was selected containing a diffraction-limited TfR-pHl punctum. An adjacent ROI of the same size containing membrane but no diffraction-limited puncta was used to calculate background intensity. The average intensity of the punctum ROI over time is plotted in green and the average intensity of the background ROI in red. The punctum intensity with the background intensity subtracted is shown in blue. Scission is indicated with a black arrow.

Please note: Wiley-Blackwell are not responsible for the content or functionality of any supporting materials supplied by the authors. Any queries (other than missing material) should be directed to the corresponding author for the article.

References

1. Doherty GJ, McMahon HT. Mechanisms of endocytosis. Annu Rev Biochem 2009;78:857–902.
2. Rappoport J, Simon S, Benmerah A. Understanding living clathrin-coated pits. Traffic 2004;5:327–337.
3. Chang HC, Newmyer SL, Hull MJ, Ebersold M, Schmid SL, Mellman I. Hsc70 is required for endocytosis and clathrin function in *Drosophila*. J Cell Biol 2002;159:477–487.
4. Boucrot E, Saffarian S, Massol R, Kirchhausen T, Ehrlich M. Role of lipids and actin in the formation of clathrin-coated pits. Exp Cell Res 2006;312:4036–4048.
5. Merrifield CJ, Feldman ME, Wan L, Almers W. Imaging actin and dynamin recruitment during invagination of single clathrin-coated pits. Nat Cell Biol 2002;4:691–698.
6. Rappoport JZ, Simon SM. Real-time analysis of clathrin-mediated endocytosis during cell migration. J Cell Sci 2003;116:847–855.
7. Rappoport JZ, Kemal S, Benmerah A, Simon SM. Dynamics of clathrin and adaptor proteins during endocytosis. Am J Physiol Cell Physiol 2006;291:C1072–C1081.
8. Ehrlich M, Boll W, van Oijen A, Hariharan R, Chandran K, Nibert ML, Kirchhausen T. Endocytosis by random initiation and stabilization of clathrin-coated pits. Cell 2004;118:591–605.
9. Loerke D, Mettlen M, Yarar D, Jaqaman K, Jaqaman H, Danuser G, Schmid SL. Cargo and dynamin regulate clathrin-coated pit maturation. PLoS Biol 2009;7:628–639.
10. Rappoport JZ, Taha BW, Lemeer S, Benmerah A, Simon SM. The AP-2 complex is excluded from the dynamic population of plasma membrane-associated clathrin. J Biol Chem 2003;278:47357–47360.
11. Puthenveedu MA, von Zastrow M. Cargo regulates clathrin-coated pit dynamics. Cell 2006;127:113–124.
12. Axelrod D. Total internal reflection fluorescence microscopy in cell biology. Biophotonics 2003;361:1–33.
13. Saffarian S, Kirchhausen T. Differential evanescence nanometry: live-cell fluorescence measurements with 10-nm axial resolution on the plasma membrane. Biophys J 2008;94:2333–2342.
14. Merrifield CJ, Perrais D, Zenisek D. Coupling between clathrin-coated-pit invagination, cortactin recruitment, and membrane scission observed in live cells. Cell 2005;121:593–606.
15. Allersma MW, Bittner MA, Axelrod D, Holz RW. Motion matters: secretory granule motion adjacent to the plasma membrane and exocytosis. Mol Biol Cell 2006;17:2424–2438.
16. Lee DW, Wu X, Eisenberg E, Greene LE. Recruitment dynamics of GAK and auxilin to clathrin-coated pits during endocytosis. J Cell Sci 2006;119:3502–3512.
17. Yarar D, Waterman-Storer CM, Schmid SL. A dynamic actin cytoskeleton functions at multiple stages of clathrin-mediated endocytosis. Mol Biol Cell 2005;16:964–975.
18. Warnock DE, Baba T, Schmid SL. Ubiquitously expressed dynamin-II has a higher intrinsic GTPase activity and a greater propensity for self-assembly than neuronal dynamin-I. Mol Biol Cell 1997;8:2553–2562.
19. Rappoport JZ, Heyman KP, Kemal S, Simon SM. Dynamics of dynamin during clathrin mediated endocytosis in PC12 cells. Plos One 2008;3:e2416.
20. Carter RE, Sorkin A. Endocytosis of functional epidermal growth factor receptor-green fluorescent protein chimera. J Biol Chem 1998;273:35000–35007.
21. Miesenbock G, De Angelis DA, Rothman JE. Visualizing secretion and synaptic transmission with pH-sensitive green fluorescent proteins. Nature 1998;394:192–195.
22. Bashkirov PV, Akimov SA, Evseev AI, Schmid SL, Zimmerberg J, Frolov VA. GTPase cycle of dynamin is coupled to membrane squeeze and release, leading to spontaneous fission. Cell 2008;135:1276–1286.
23. McNiven MA, Cao H, Pitts KR, Yoon Y. The dynamin family of mechanoenzymes: pinching in new places. Trends Biochem Sci 2000;25:115–120.
24. Roux A, Uyhazi K, Frost A, De Camilli P. GTP-dependent twisting of dynamin implicates constriction and tension in membrane fission. Nature 2006;441:528–531.
25. Sever S, Damke H, Schmid SL. Garrotes, springs, ratchets, and whips: putting dynamin models to the test. Traffic 2000;1:385–392.
26. Eisenberg E, Greene LE. Multiple roles of auxilin and Hsc70 in clathrin-mediated endocytosis. Traffic 2007;8:640–646.
27. Massol RH, Boll W, Griffin AM, Kirchhausen T. A burst of auxilin recruitment determines the onset of clathrin-coated vesicle uncoating. Proc Natl Acad Sci U S A 2006;103:10265–10270.
28. Fujimoto LM, Roth R, Heuser JE, Schmid SL. Actin assembly plays a variable, but not obligatory role in receptor-mediated endocytosis in mammalian cells. Traffic 2000;1:161–171.
29. Benmerah A, Lamaze C. Clathrin-coated pits: vive la difference? Traffic 2007;8:970–982.
30. Heuser J. Three-dimensional visualization of coated vesicle formation in fibroblasts. J Cell Biol 1980;84:560–583.
31. Kner P, Chhun BB, Griffis ER, Winoto L, Gustafsson MG. Super-resolution video microscopy of live cells by structured illumination. Nat Methods 2009;6:339–342.
32. Rappoport JZ, Simon SM. Endocytic trafficking of activated EGFR is AP-2 dependent and occurs through preformed clathrin spots. J Cell Sci 2009;122:1301–1305.
33. Pucadyil TJ, Schmid SL. Real-time visualization of dynamin-catalyzed membrane fission and vesicle release. Cell 2008;135:1263–1275.
34. Zacharias DA, Violin JD, Newton AC, Tsien RY. Partitioning of lipid-modified monomeric GFPs into membrane microdomains of live cells. Science 2002;296:913–916.
35. Jouvenet N, Bieniasz PD, Simon SM. Imaging the biogenesis of individual HIV-1 virions in live cells. Nature 2008;454:236–240.